A design analysis of vertical stabilisers for Blended Wing Body aircraft

Geoffrey Larkin[a], Graham Coates[a,*]

[a]*School of Engineering and Computing Sciences, Durham University, South Road, Durham, DH1 3LE, UK*

Abstract

Blended Wing Body (BWB) aircraft are a relatively new concept offering advantages of aerodynamic performance and fuel economy. In BWB aircraft design, directional stability has been identified as one aspect that remains under-researched. This paper presents a design analysis of vertical stabilisers on a BWB aircraft to determine their suitability and effects on stability. Founded on an existing model [1], a baseline BWB aircraft model has been developed with vertical stabilisers designed using the volume coefficient method which, although not created for BWB aircraft, is used to aid the design. To ensure suitability for transonic flight, stabiliser dimensions were kept in proportion to that of the Airbus A380 due to having a similar payload and cruise condition. Two BWB aircraft CAD models were developed; one with twin-stabilisers mounted vertically and another with them inclined. CFD analyses were performed to assess stability with respect to rudder inputs and sideslip angle. Stability derivatives calculated were similar for both twin-stabiliser configurations; however, the inclined configuration gave a smoother response. Drag performance was also assessed with the inclined stabilisers generating greater drag than the vertical stabilisers. This research has shown that a twin-stabiliser design is suitable for BWB aircraft.

Keywords: Aircraft design, blended wing body; vertical stabilisers; stability

*Corresponding author.
Email address:* `graham.coates@durham.ac.uk` (Graham Coates)

1. Nomenclature

Symbols

AR	Aspect ratio
b	Wingspan (m)
C_D	Drag coefficient
C_L	Lift coefficient
C_l	Rolling moment coefficient with reference to wingspan
C_{l_β}	Rolling moment coefficient derivative with respect to sideslip angle
$C_{l_{\delta r}}$	Rolling moment coefficient derivative with respect to rudder angle
C_m	Pitching moment coefficient with reference to mean aerodynamic chord
C_{m_β}	Pitching moment coefficient derivative with respect to sideslip angle
$C_{m_{\delta r}}$	Pitching moment coefficient derivative with respect to rudder angle
C_m	Yawing moment coefficient with reference to wingspan
C_{n_β}	Yawing moment coefficient derivative with respect to sideslip angle
$C_{n_{\delta r}}$	Yawing moment coefficient derivative with respect to rudder angle
CP	Centre of pressure (m)
C_r	Root chord of tail (m)
C_{rudder}	Rudder chord (m)
C_t	Tip chord of tail (m)
C_{vt}	Vertical volume coefficient
$F_{x_{vt}}$	Tail force in positive x direction (N)
$F_{y_{vt}}$	Tail force in positive y direction (N)
$F_{z_{vt}}$	Tail force in positive z direction (N)
h	Vertical stabiliser height (m)
L	Rolling moment (Nm)
l_{vt}	Tail arm (m)
l_x	Longitudinal moment arm (m)
l_y	Vertical moment arm (m)
l_z	Horizontal moment arm (m)
M	Pitching moment (Nm)
MAC	Mean aerodynamic chord (m)
N	Yawing moment (Nm)
q	Dynamic pressure (Pa)
S_{vt}	Vertical stabiliser area (m^2)
SF	Scaling factor
S_w	Trapezoidal wing area (m^2)

U	Velocity vector (m/s)
V_{mcg}	Minimum controllable ground velocity (m/s)
X	Longitudinal distance (m)
Z_T	Engine spanwise location (m)
α	Angle of attack (°)
β	Sideslip angle (°)
δ_r	Rudder angle (°)
Λ_{LE}	Leading edge sweep angle (°)
Λ_{TE}	Trailing edge sweep angle (°)
λ	Taper ratio
ϕ	Angle of inclination (°)

Subscripts

MAC	Mean aerodynamic chord
o	Value at zero sideslip and rudder angle
p	Port vertical stabiliser
s	Starboard vertical stabiliser
vt	Vertical tail
w	Trapezoidal wing area
wb	Wing & body section

2. Introduction

The volume of air traffic in the United Kingdom (UK) has increased by 130% between 1990 and 2008 [3]. Gains in fuel efficiency have been sought by using lightweight structural composites such as carbon-fiber-reinforced plastic frames as used in the Airbus A380 [4]. Boeing's Subsonic Ultra Green Aircraft Research (SUGAR) project improved aerodynamic efficiency through increasing wingspan [5], which increases the aspect ratio and hence reduces induced drag. Aircraft designers could continue increasing wingspan or reducing weight using the traditional tube-and-wing configuration but there are limitations such as material strength and the maximum wingspan to fit in Class 5 airports' 80m box [6]. Alternative configurations such as the BWB could make significant steps towards reaching the Advisory Council for Aeronautical Research in Europe's (ACARE) target of reducing fuel consumption and CO_2 by 50% per passenger kilometre by 2020, compared with data from 2000 [7].

The BWB design configuration blends the main fuselage in to the wing as illustrated in Figure 1a giving a larger fuselage section thus reducing the ratio of wetted area to wingspan and hence skin friction drag. The main body is shaped as an aerofoil, rather than a tube, so extra lift can be generated on this section, whilst engines can be mounted on top of the main body to help reduce noise levels. The concept of the BWB aircraft date back to the Westland Dreadnought of 1924 [8] and the Miles M.30 of 1942 [9]. However, it received renewed interest for transport and civil applications in 1988 when NASA Langley research centre funded a small study with McDonnell Douglas to investigate the performance potential of the configuration for a range of 7000n-mile with 800 passengers at a cruise Mach number of 0.85 [10].

The European Commission has funded a series of projects between 2000 and 2012 dedicated to research in to various aspects of the BWB concept [11]. Throughout these 13 years of research, depending on the aims of the individual project, the designs used have varied greatly in terms of body shape, engine configuration and tail configuration. Running from 2000 to 2003, the first project was the Multidisciplinary Optimization of a Blended Wing Body (MOB) project, which generated a baseline BWB design configuration [11]. From 2002 to 2005, the Very Efficient Large Aircraft (VELA) project was, as its name suggests, aimed at making large aircraft very efficient. The output of this project was a 4-engined, twin tail aircraft design with no winglets [12]. One of the problems highlighted in this project was the lack of simulation methods specific to BWB aircraft [11]. The Silent Aircraft Initiative, launched in 2003 and ending in 2006, was a collaboration between Massachusetts Institute of Technology and the University of Cambridge. This project was aimed at producing aircraft with reduced noise output and led to the design of the Silent Aircraft Experimental, SAX-40, which made use of three aft-mounted ducted engines, a highly curved main body and angled winglets in a tailless configuration [13]. The New Aircraft Concepts Research (NACRE) project ran from 2005 to 2009. Two 'Pro Green' concepts were developed which used a traditional tube-and-wing configuration but investigated the potential of advanced wing designs to reduce fuel burn and novel tail designs to reduce noise [14]. A flying wing concept was also considered, which used the geometry from the VELA project, however placed a focus on environmental friendliness, emergency egress and passenger comfort [14]. This project also addressed the issues caused by locating the propulsion systems aft of the aircraft's centre of gravity [11]. The most recent project was the Active Control for Flexible Aircraft (ACFA) 2020 project, which

ran from 2008 to 2011. The BWB aircraft designed had two pod-mounted engines at the aft of the main body, large winglets and no tail. Further, this project designed in-flight control systems to reduce structural loads and improve passenger comfort [15].

This remainder of this paper is organised as follows. In Section 3, an overview is presented of work related to the controllability of BWB aircraft, paying particular attention to the tail arrangements of previous BWB aircraft in order to explain the rationale for the research reported in this paper. Section 4 describes the generation of the computational baseline aircraft model and choice of CFD solver used in this research. In Section 5, an introduction to the volume coefficient method is provided which is then used to aid the design of the vertically mounted twin-tails. In addition, an overview is given of the method used for designing the rudder control surfaces. Furthermore, this section determines the minimum size of tail allowable on the BWB model using a mock asymmetric thrust test. Section 6 explains the design method used for the inclined twin-tail configuration. Following this, Section 7 discusses the results of the stability analyses for the inclined and vertically mounted twin-tails, then Section 8 summarises the results of the drag analysis. Finally, Section 9 concludes the paper.

3. Related work: Controllability of Blended Wing Body aircraft

Some of the key challenges in controllability of BWB aircraft have been summarised by Kozek and Schirrer [11] as:

- "The open-loop behaviour may even be unstable due to the missing empennage and the centre of gravity location;

- Rotation at take off;

- Short moment arm for movables and control surfaces that represent a challenge for stability and control, both longitudinal and laterally;

- Current design methods widely based on conventional tube-and-wing aircraft configurations and only partially transferable to BWB aircraft."

Liebeck [10] provides an overview of the various design options to aid controllability of BWB aircraft including a reflexed main body for pitch trim and rudder surfaces that are combined in to the winglets. Liebeck states that

5

"tailless configurations have short moment arms for pitch and directional control", though this issue is true for configurations using tails as well. This means rudders and elevators will not have the same level of command as they would on a traditional tube-and-wing configuration. To overcome this issue, control surface dimensions can be increased to give larger moments, but the corresponding hinge moment will increase with the cube of the scale [10].

Lehmkeuler et al. [16] conducted a study in to the design and testing of an unmanned BWB aircraft with a twin-tail configuration. The control derivatives were measured in a wind tunnel and compared against computationally predicted values. The derivative of the yawing moment coefficient (C_n) with respect to sideslip angle (β), C_{n_β}, provides a measure of the inherent directional stability of an aircraft. A larger value means there is a greater restoring moment to revert the aircraft from a state of sideslip. Lehmkeuler reported a C_{n_β} value of 0.0365 rad^{-1} [16] which is lower than the recommended value of 0.05 rad^{-1} [17]. However, increasing tail sizes can increase this value by providing a greater restoring moment against sideslip.

The AC 20.30 BWB aircraft has been developed with a twin tail configuration along with winglets and two engines [18]. For this aircraft, Neubacher uses stability derivatives obtained from wind tunnel testing to model the dynamic motion of the aircraft using Matlab's Simulink package. The stability derivatives given were a C_{n_β} value of 0.0344 rad^{-1}, a C_{l_β} value of -0.1031 rad^{-1} and a $C_{n_{\delta r}}$ value of -0.0130 rad^{-1} at a Mach number of 0.06 and angle of attack of 2°. The sign of these values of stability derivatives imply that the AC 20.30 aircraft is directionally statically stable. This means that the restoring moments produced by the aircraft due a perturbation in flight act in the correct direction. A detailed explanation of the conditions for an aircraft to be considered directionally stable is provided in Section 7.1 Neubacher concludes that the AC 20.30 is dynamically unstable for the spiral mode, but dynamically stable for both the dutch roll and roll mode [18]. Whilst an aircraft must be statically stable in order to be dynamically stable, achieving static stability does not imply that dynamic stability has also been achieved. That is, static stability requires that the restoring moments act in the correct direction whereas dynamic stability is dependent on the damping of these forces.

The Boeing X-48 project was conducted in the United States between 2004 and 2013 in conjunction with NASA [19]. The first aircraft version of this project, the X-48A, was abandoned before flight testing. Following this the second configuration, the X-48B, was flight tested though suffered from

6

pitch tumble when a certain angle of attack was exceeded [20]. The X-48C was modified by removing the winglets and adding twin-vertical stabilisers further inboard on either side of the engines to create a low-noise version [21].

Each project referred to thus far, summarised in Table 1, has focused on a particular design aspect of BWB aircraft. Pitch stability has often been prioritised in order to optimise the shape of a BWB, as in the work of the MOB project [1], and also because there has been a need to better understand unique effects of the design configuration such as pitch tumble reported in the Boeing X-48 projects [20]. In part, this has led to a lack of data being published regarding directional stability for BWB aircraft. This is also a problem due to the BWB design configuration still being in its infancy with no commercial BWB aircraft having been produced to date. Furthermore, projects such as the X-48 projects are commercially oriented so it is not possible to obtain numerical data from the flight testing.

In the projects referred to in Table 1, the tail and winglet arrangements vary between designs with some opting for a twin-tail configuration and some for a tailless configuration. The range of design choices indicates that there is no consensus as to whether tailless or twin-tail configurations are more suitable for BWB aircraft. Even in projects such as VELA [12] which used tails, no published data could be found as to the design methods used or the performance of the tails once installed on a BWB aircraft. Table 1 also highlights that there is no trend with time towards the use of a tailless or twin-tail configuration, which may have suggested that one design could be outperforming the other.

The aim of the design analysis presented in this paper is to investigate the directional stability characteristics of twin-tail design configurations applied to a BWB aircraft. This will give guidance for the use of tails on BWB aircraft, both in terms of their feasibility and their performance, whilst also informing how traditional design methods should be adapted to suit this contemporary design configuration. Firstly, the issue of short moment arms for tails and control surfaces must be addressed to determine whether practically sized tails can be developed for the BWB design configuration.

Project	Years	Tail arrangement	Winglet arrangement
Multidisciplinary Optimization of a BWB [1]	2000-03	Tailless	No Winglets
Very Efficient Large Aircraft [12]	2002-05	Twin-tail	No Winglets
Silent Aircraft Initiative [13]	2003-06	Tailless	Angled
New Aircraft Concepts Research [14]	2005-09	Twin-tail	No Winglets
Active Control Flexible Aircraft [15]	2008-11	Tailless	Winglets
X-48B [20]	2005-10	Tailless	Winglets
X-48C [21]	2009-13	Twin-tail	No Winglets

Table 1: Configurations for BWB projects [1], [12], [13], [14], [15], [20], [21]

4. Baseline model of a Blended Wing Body aircraft: Geometry and solver validation

The baseline CAD model developed and used in this research is based on geometry and aerofoil plots given by Qin et al. [1] as part of the MOB project. Aerofoils at the spanwise locations shown in Figure 1a were created by taking discrete points from the thickness distributions given in Figure 1b. Note that the baseline model lies in the x-z plane, making z the horizontal direction. Lofted surfaces were then interpolated between the aerofoils. Winglets were added using NACA0012 aerofoils, as used in [1], which are 3m high and stretch from 37.5m to 39.35m span thus allowing the aircraft to fit in the 80m box for Class 5 airports [6].

The baseline model, shown in Figure 1a, has a planform area of 1491m^2. Neglecting the winglets, the trapezoidal wing area (S_w) is 873m^2 with a mean aerodynamic chord (MAC_w) of 12.8m. As in [1], the aircraft's centre of gravity location, which is used in torque calculations, has been set at 29.3m in the longitudinal direction from the aircraft nose. Table 2 gives the chord length (C) at each spanwise station, along with the longitudinal distance (X) from the nose of the aircraft to the leading edge of the wing at that station.

The aerodynamic modelling in this research has been conducted using 'Solidworks Flow Simulation' [2], which is a CAD-embedded CFD package. Conveniently, this allows the CAD model to be generated and meshed within one package, so control surfaces can be adjusted and automatically re-meshed. The immersed-body mesh divides cells in to fluid and solid re-

Span-wise station (m)	C (m)	X (m)
0	50.8	0
13.0	23.07	27.73
17.5	14.51	31.25
23.5	9.72	35.96
38.75	4.02	47.85
39.35	1.29	51.55

Table 2: Chord length, C, and longitudinal distance, X, from aircraft nose to leading edge of spanwise stations

gions, rather than just meshing the fluid domain, which allows the aircraft geometry to be captured using a relatively coarse mesh. To solve turbulent flows the Favre-averaged Navier-Stokes equations are used with the k-epsilon model to close the equations [22]. Furthermore, different approaches are used for thin and thick boundary layers. For thin boundary layers, where the number of cells is not sufficient to capture the flow, a Prandtl approach is used [22]. For thick boundary layers with turbulent flow, a wall function approach is used with the full velocity profile proposed by Van Driest in 1956, rather than the typical logarithmic profile, in order to better model the near-wall relationship [22]. Laminar flow in thick boundary layers can be solved directly as part of the core fluid [22]. Verifications of the Solidworks Flow Simulation boundary layer treatment have been completed by Balakin et al. using both fundamental tests and industrial applications, which concluded that very good agreement was obtained between numerical and experimental data [23], and thus confirms the validity of the choice of CFD solver used in this design analysis.

In order to ensure the suitability of the baseline model developed in this research being analysed with Solidworks Flow Simulation, a lift and drag polar diagram was created to compare the results of the baseline model with those presented by Qin et al. [1]. This comparison was conducted at the conditions for which the aircraft was designed, specifically an altitude of 11500m, cruise Mach number of 0.85 and cruise speed of 250.8m/s [1]. Figure 2a shows the values for lift and drag coefficient for the baseline model and the model presented by Qin et al. [1] as the angle of attack (α) is varied between 1.75° and 5°.

The percentage differences between the baseline model's lift and drag coefficients at different angles of attack and that of Qin et al.'s model are presented in Table 3. The baseline model consistently gives lower lift coefficients than those of Qin et al.'s model. However, the lift coefficients agree to within 2.4% at an angle of attack of 5°. The baseline model gives lower drag than Qin et al.'s model for an angle of attack greater than or equal to 3°. The differences can be accounted for by the discrete method used to create the aerofoils which produces a less cambered aerofoil, and hence a lower lift coefficient. As this research is entirely independent of the results presented by Qin et al., it was not considered necessary for the results for the two models to be identical. Importantly, the results for the baseline model followed the same trend as that of Qin et al., as shown in Figure 2a, confirming that inputs to the CFD solver are producing the expected changes in flow around the aerofoil sections. The results obtained were therefore considered acceptable to continue testing with the combination of 'Solidworks Flow Simulation' and the baseline model.

α (°)	C_L	C_D
1.75	-12.0	36.1
3	-17.3	-2.2
4	-17.5	-12.4
5	-2.4	-11.9

Table 3: Percentage differences between Qin et al.'s model [1] and the baseline model

Eight levels of mesh refinement are available in Solidworks Flow Solver with level 1 and level 8 being the least and most refined respectively. A higher level of refinement increases solution accuracy while at the same time causes the solver to take more time to converge at each iteration. Whilst Solidworks Flow Solver's auto-refinement feature automatically refines the mesh if the solver is unable to converge to a final solution after a set number of iterations, a mesh refinement study was required in order to determine which level of refinement to use when initiating simulations. This study was conducted at an angle of attack of 4° since the baseline model was closest to achieving Qin et al.s' model lift coefficient of 0.41 at this angle. In Figure 2b, the percentage change in lift and drag of the baseline model between the

current and previous level of refinement are plotted, e.g. the results for level 5 show the change when increasing mesh refinement from level 4 to level 5. Figure 2b focuses on levels 5 to 7 as (i) the solver automatically refined to at least level 4 in trial simulations, and (ii) level 7 only gave a change of 1.75% for lift and 0.87% for drag when compared with level 6. The values in Figure 2b indicate that the accuracy of level 5 is within that of the discrete method used to plot the aerofoils of the baseline model, quantified by the percentage differences in performance between the baseline model and the model of Qin et al., at an angle of attack of 4°, presented in Table 3. Thus, level 5 was selected as the initial refinement level for simulations. Furthermore, level 5 offered an acceptable compromise between solution accuracy and time to solution.

5. Vertically mounted twin-stabiliser design

This section introduces the volume coefficient design method which is traditionally used to size vertical stabilisers. The design of the twin-stabilisers by use of the volume coefficient method is then detailed, along with the design of their control surfaces, leading to the production of a family of vertically mounted twin-stabilisers (see Figure 3) for consideration on the baseline model. Subsequently, in Section 5.4, this family of stabilisers is examined to determine the minimum size of stabiliser that can be safely installed on the baseline model whilst incurring the least effect on aircraft drag. Following this, the baseline model, with the minimum allowable size of stabilisers attached, is analysed in terms of stability and drag performance in Sections 7 and 8 respectively.

5.1. Volume coefficient method

The volume coefficient method is used in scoping calculations for sizing an aircraft's vertical stabilisers [17], also referred to as tails. Whilst this method is not a novel method created specifically for the BWB design configuration, using it allows an acceptable range of the volume coefficient to be obtained that is suitable for the BWB design configuration. This method relates the tail area to the wing area. The value of tail area, S_{vt}, is determined using equation (1), where C_{vt} is the vertical volume coefficient, b is the wingspan and S_w is the trapezoidal wing area. In this research, C_{vt} is also referred to simply as the volume coefficient since no horizontal control surfaces are modelled.

11

$$S_{vt} = \frac{C_{vt}bS_w}{l_{vt}} \tag{1}$$

Also, in equation (1), l_{vt} is the tail arm, i.e. the distance between the centres of pressure of the wing and the vertical tail, CP_w and CP_{vt} respectively. The centres of pressure are taken to act at the quarter-chord point on their respective mean aerodynamic chords [17]. This position corresponds to the aerodynamic centre for symmetric aerofoils [17] and is highlighted in Figure 4. This decision was made so that any aerodynamic moments arising on the tails will not vary with sideslip angle, and therefore can be discounted in the stability analysis of the tails with respect to sideslip. The moment arm of the tail in the longitudinal direction acts between CP_{vt} and the aircraft centre of gravity location, and will be differentiated from l_{vt} by the use of l_x.

There is a trade-off between size of tail and its moment arm since a greater value of C_{vt} yields a larger tail area and therefore greater horizontal forces; however as the rear of the tail is fixed by the aircraft length, increasing C_{vt} also reduces the tail arm. Although the reduction in tail arm is small in comparison to the increase in tail area, this constraint does penalise larger tails as it reduces the effectiveness of the tail in producing restoring moments.

The vertical volume coefficient of an A380 has been calculated to be 0.05967 [24]. If this value was applied to the baseline BWB model with a single tail, it would yield a tail side-view area of 282m^2, which is 2.1 times larger than the area of the tail used on an A380 at 134m^2 [24]. Even using a twin-tail configuration with this value of volume coefficient would yield tails of 141m^2 each. These would extend 14.1m along the main body, negating the lift and capacity benefits of the BWB design. These scoping calculations show that for the BWB design configuration a twin-tail design must be used with a reduced volume coefficient compared with current large aircraft. If this is not the case, then it would be unfeasible to design BWB aircraft with tails and a tailless design must therefore be used.

5.2. Design method for vertically mounted twin-tails

A family of tails shown in Figure 3 was created for use on the baseline model in a vertically mounted twin-tail configuration, as seen in Figure 6. They were generated using NACA0012 aerofoils as tail aerofoils should be symmetric about the chord line [25]. The volume coefficient method was used but with values of volume coefficient less than that of an A380. When

12

creating twin-tail designs, equation (1) is still used as for a single tail design, but the calculated area is then divided equally between the two tails.

An initial estimate of tail arm and choice of volume coefficient was required in order to obtain the vertical stabiliser area from equation (1). As the tail arm is dependent on the location of CP_{vt}, which is itself dependent on the tail dimensions, the initial tail arm is set as the distance between the rear of the aircraft and CP_w. Once the dimensions of the tail are defined, the tail arm and volume coefficient can be recalculated to find their updated values. Figure 4 provides a side view of a tail with its associated dimensions.

The dimensions of the tails were kept in proportion to those of the A380 tail in order to ensure their suitability for transonic flight. This was achieved by multiplying the root chord (C_r), tip chord (C_t) and height (h) of the A380 tails [24] by the scaling factor, SF, defined in equation (2),

$$SF = \sqrt{\frac{S_{vt\ (BWB)}}{S_{vt\ (A380)}}} \qquad (2)$$

Defining the tail design method in this way gave commonality for testing as it kept the aspect ratio (AR) and taper ratio (λ) constant at 1.39 and 0.424 respectively for any choice of volume coefficient, as on the A380 tail. The trailing edge sweep angle (Λ_{TE}) was set at a constant 17.9° as used on the A380 [24]. This combination of design choices gave a leading edge sweep angle (Λ_{LE}) of 42.14° for all cases, within the recommended limits of 35° and 55° [17], ensuring suitability for transonic flight.

The tails were mounted vertically either side of the aircraft centre-line at a spanwise distance of 13m where the main body meets the inner wing, shown in Figure 1a. This would give the largest possible clearance from engine wake whilst still allowing the tails to be mounted on the structure of the main body. The tails' trailing edges were set coincident with the trailing edge of the aircraft and the root of the tails were set coincident with the y=0 plane (the vertical centreline) of the aircraft model, so that a small portion of the tail is embedded within the aircraft body.

5.3. Design method for rudder control surfaces

A single control surface was used for the rudder of each tail. The chord of the rudder (C_{rudder}) has been defined as 25% of the average tail chord. This gives a conservative estimate of potential rudder forces as the rudder chord is advised to equal 25-50% of the tail chord [17]. This choice gave a rudder

which was triangular in shape with a maximum width of 0.45m, equal to the tail thickness at that point. Fillets of 0.2m were added at the leading edge, highlighted in Figure 4. The rudder extended from the base of the tail up to 90% of the trailing edge length. The rudder rotated about an axis parallel to the tail's trailing edge which, in order to minimise hinge moments [17], was positioned at 80% of the distance from the trailing edge to the leading edge of the rudder.

5.4. Sizing of the vertical stabilisers using asymmetric thrust testing

This section determines the minimum allowable size of vertical stabiliser for use on the baseline model from the family of vertically mounted twin-tails described in Section 5.2, and hence suggest a suitable range of C_{vt} for BWB aircraft. In order to do this, CFD software was used to perform a 'mock' asymmetric thrust test as this represents a worst-case scenario of yawing moments that the tails must be able to counteract. This situation can occur during take-off if the engine(s) on one side of the aircraft fail. The test was conducted in accordance with the European Aviation Safety Agency (EASA) Certification Specifications chapter 25.149 [26]. These require that the test is carried out with:

- the most critical engine failure considered (i.e. furthest outboard);

- maximum available take-off power or thrust on the operating engines;

- the aircraft travelling at the minimum controllable ground speed (V_{mcg});

- rudders engaged at full deflection.

The minimum control speed on the ground, V_{mcg}, is the minimum calibrated airspeed during the take-off run at which, when the critical engine is suddenly made inoperative, it is possible to maintain control of the aeroplane using rudder control alone [26]. As rudder force increases with speed, this is the most critical condition for the rudder to resist the moment from asymmetric thrust. Numerous tests would be required to find the exact value of V_{mcg} for the BWB model. Therefore, the value of V_{mcg} of an A380, which is equal to 66.88 m/s [27], has been used at ground conditions of 101.3kPa and 293K [17]. The maximum rudder engagement (δ_r) of an A380 is 30° [28] so this angle has been applied to the rudders on both of the vertical stabilisers

for testing. In accordance with convention, positive rudder engagement is defined as the trailing edge of the rudder moving to port.

The yawing moments resulting from an engine failure have been calculated for configurations with engines located at different spanwise distances, Z_T, from the aircraft centreline. These were calculated using the maximum thrust (348.31kN) of a single Rolls Royce Trent 970B-84 engine, as used on an A380-841-000 [28]. Most BWB designs to date, including the X-48B [20] and SAX-40 [13] aircraft, have used two or three engines symmetrically mounted about the centreline of the aircraft. For these configurations, even in the event of two engine failures, there would be a maximum of one engine contributing to the asymmetric thrust moment. The tail yawing moments were calculated as the product of the horizontal tail force, $F_{z_{vt}}$, and its longitudinal moment arm, l_x. The yawing moments resulting from asymmetric thrust, as well as from both tails combined, are shown in Figure 5.

The tails with a volume coefficient of 0.02417 (40.5% of that used for an A380) will be used for all further testing as they were the smallest tails which produced a sufficient yawing moment to counteract the thrust from an engine located 7m from the centreline, seen at point 'A' in Figure 5. Using this value of volume coefficient, along with the design choices outlined in Section 5.2, yields vertical tails of height 10.85m, root chord 10.96m and tip chord 4.65m. The model with this size of tail is illustrated in Figure 6. This size of tail is also highlighted in Figure 3 for comparison with the other tails tested. Therefore, the reduction of volume coefficient by 59.5% on the A380, which is representative of current large aircraft, is suggested for twin-tail BWB aircraft designs.

As the aircraft is at zero sideslip angle during the asymmetric thrust testing, the lift coefficient of the vertical tails, $C_{L_{vt}}$, is given by [17]

$$C_{L_{vt}} = \frac{F_{z_{vt}}}{qS_{vt}} \tag{3}$$

where q is the free-stream dynamic pressure. The lift coefficient of the vertical tails is plotted against volume coefficient in Figure 5. As the tails with a volume coefficient of 0.0138 yield the highest lift coefficient of 0.393, seen at point 'B' in Figure 5, they are the most effective of the tails at 30° rudder engagement. However, these tails do not generate a sufficient moment to counteract the asymmetric thrust considered, even with the engines mounted at 6m from the centreline as can be seen from the blue line lying underneath the bottom dashed black line at this value of volume coefficient in Figure 5.

15

However, this value could be utilised on aircraft with smaller payloads and thrust requirements in order to minimise tail area, achieving weight and drag reduction.

6. Inclined mounted twin-stabiliser design

This section describes adjustments made to the design method presented in Section 5, which was used to produce a family of vertically mounted twin-stabilisers for consideration on the baseline model, in order to produce an inclined mounted twin-stabiliser design for a BWB aircraft. Also, a summary is given of a sensitivity study undertaken to determine at what angle the inclined twin-stabilisers should be mounted. The inclined mounted twin-stabiliser design, along with the vertically mounted twin-stabiliser design, are then analysed in terms of stability and drag performance in Sections 7 and 8 respectively.

For the analysis of tail stability, both the vertically mounted configuration (see Figure 6) and inclined mounted configuration (see Figure 7) of twin-tail design will be analysed using a vertical volume coefficient of 0.02417, which was found to be acceptable according to the asymmetric thrust test of the vertically mounted twin-tail design described in Section 5.4. The same value of volume coefficient can also be used for the inclined mounted twin-tail design in order to set the vertically projected area of the tails, which horizontal forces are proportional to, rather than the total tail areas. The angle of inclination, ϕ, measured from the vertical was, initially, set arbitrarily (but then determined later in this section), allowing the total tail area to be calculated from the vertically projected area. The design process of the tail is then repeated as described in Sections 5.2 and 5.3, except that the total tail area is now used to scale dimensions using equation (2).

As the design method used for the inclined tails fixes the vertically projected area, the total tail area is inversely proportional to $\cos(\phi)$, as can be deduced trigonometrically from Figure 7. However, the horizontal force generated by the tails is directly proportional to both the total tail area (as pressure forces are proportional to area) and $\cos(\phi)$ (to resolve the forces in to the horizontal direction). Therefore, these relationships are expected to counteract each other giving a horizontal force, and hence yawing moment, which is independent of the angle of inclination. Although increasing the angle of inclination increases the tail area and therefore also reduces the tail arm

16

(as mentioned in Section 5.1), the range of angles tested was relatively small (15° to 25°) so the effect on yawing moments was expected to be minimal.

A sensitivity study has been conducted for angles of inclination ranging from 15° to 25° to determine whether the assumption that yawing moments are independent of the angle of inclination is reasonable. The study was conducted at the design conditions of altitude 11500m, a cruise Mach number of 0.85 and cruise speed of 250.8m/s [1] as these are also used for the stability analysis in Section 7. The rudders were engaged to 10° on both tails to avoid non-linear effects - engaging the rudders up to their maximum engagement of 30° could cause them to stall, falsely indicating poor performance. There was no obvious trend in yawing moments with angle of inclination. However, the tails inclined at 22° from the vertical gave the largest yawing moment, and have therefore been used as the inclined configuration in all further analysis. This yielded inclined tails with a height of 11.26m (in the plane of the tail), root chord 11.38 and tip chord 4.83m.

7. Design assessment: Stability analysis

In this section, the theory of lateral and directional stability is introduced; both how it is quantified and the requirements for it to be achieved. Following this, an explanation is given as to how this theory is adapted for the baseline model and how the quantities have been determined from the computational experimentation. The results with respect to sideslip and rudder angle are then presented for both the vertical and inclined tail configurations.

7.1. Analysis methodology

The vertical and inclined twin-tail configurations have been analysed for their directional and lateral stability at the aircraft cruise conditions of altitude 11500m, a cruise Mach number of 0.85 and cruise speed of 250.8m/s [1]. They have also been analysed for their stability with respect to rudder inputs. Static stability defines the aircraft's ability to provide a restoring force which will act to return the aircraft to trimmed conditions after a perturbation such as a change in velocity direction. Figure 8 indicates the convention of positive aerodynamic moments, where L, M and N are the rolling, pitching and yawing moments respectively. Figure 8 also shows the direction of the positively defined cartesian axes used in this research in order to align with the CFD output.

In order to use standard equations (5) to (10), which are defined later in this section, and be able to compare with data from other aircraft, rolling, pitching and yawing moment coefficients will be used, defined respectively as stated in [17]

$$C_l = \frac{L}{qS_wb}, \;\; C_m = \frac{M}{qS_wMAC_w}, \;\; C_n = \frac{N}{qS_wb} \;\; . \tag{4}$$

Stability derivatives are then defined as the derivative of a moment coefficient with respect to a change in flow conditions or a control surface input. These provide a measure of how responsive the aircraft is to an input and how stable it is.

Taking the derivative of yawing moment coefficient with respect to sideslip angle, C_{n_β}, gives the directional (sometimes called weathercock) stability. For an aircraft to be stable it should rotate in to the oncoming air. Therefore a positive sideslip angle, defined as velocity vector approaching from starboard of the nose (highlighted in Figure 8), should give rise to a positive yawing moment. Hence for the aircraft to be stable, C_{n_β} must be positive [25].

As both tails' centres of pressure lie above the aircraft's centre of gravity in both the inclined and vertical configurations, horizontal tail forces will produce a rolling moment, so coupling between yawing and rolling moments is expected. Rolling moments are defined as positive if they cause the starboard wings to roll downwards. For lateral stability to be achieved, the derivative of rolling moment coefficient with respect to sideslip angle, C_{l_β}, should be negative so that the aircraft rolls away from the sideslip, and is advised to be about half of C_{n_β} in magnitude at subsonic speeds [17]. This is known as the dihedral effect [25] as it produces the same effect as adding dihedral to wings. If the value becomes overly negative, the aircraft will suffer from dutch roll mode where it oscillates in a circular motion when viewed from behind; however a positive value would cause the plane to spiral when entering a sideslip. The change in pitching moment with respect to sideslip should be minimised for the plane to behave predictably.

Positive rudder inputs (positive to port) should produce a negative yawing moment, so the derivative of yawing moment coefficient with respect to rudder input, $C_{n_{\delta r}}$, must be negative for stability [25]. Positive rudder inputs will induce positive rolling moments away from the intended direction of yaw rotation. These rolling moments should be minimised to avoid the pilot having to apply excessive aileron control to counteract them. The change in pitching moment with respect to rudder input should also be minimised to

avoid the need for further control inputs.

Raymer [17] presents equations for C_{l_β}, C_{m_β} and C_{n_β}, which have been modified to make them suitable for application to the model presented in this paper. These modified equations are presented in equations (5) to (7), where i can be interpreted as l, m or n for rolling, pitching and yawing axes respectively. The wing and body terms were collected as one component, denoted by 'wb' in equations (5) and (6), as their moments were output directly from the CFD simulations. Control surface terms such as ailerons which were not modelled are neglected. Terms for thrust, engine drag and air turning at engine inlet are neglected as the engines have not been modelled. If the engines had been modelled, the thrust and drag terms would have had no effect on directional stability due to their symmetrical mounting about the aircraft centreline. Finally, the port and starboard stabilisers are treated as two separate terms, denoted by p and s respectively, whereas Raymer presumes the use of only one stabiliser.

Equation (5) highlights how C_{l_β}, C_{m_β} and C_{n_β} for the whole aircraft are calculated by summing the contributions from each aircraft component,

$$C_{i_\beta} = C_{i_{\beta_{wb}}} + C_{i_{\beta_{vt(p)}}} + C_{i_{\beta_{vt(s)}}} \quad . \tag{5}$$

Similarly, the change in moment coefficient with respect to rudder angle is written as

$$C_{i_{\delta r}} = C_{i_{\delta r_{wb}}} + C_{i_{\delta r_{vt(p)}}} + C_{i_{\delta r_{vt(s)}}} \quad . \tag{6}$$

The derivatives can then be summated linearly to give the total moment coefficient [25],

$$C_i = C_{i_o} + C_{i_{\delta r}} \delta_r + C_{i_\beta} \beta \quad . \tag{7}$$

The quantities C_{l_o}, C_{m_o} and C_{n_o} are the values of the moment coefficients with zero sideslip and rudder engagement. Presuming the aircraft is symmetric about the x-z plane, C_{n_o} and C_{l_o} can be assumed to be zero [25]. However, C_{m_o} is a function of angle of attack.

7.2. Calculation of moments and stability derivatives

To calculate the moments, from which stability derivatives are determined, CFD simulations have been performed at angles of rudder engagement up to 30° and sideslip angle up to 15°, all at zero angle of attack. The

moments and derivatives for each tail, the main wing and body section, and all three of these 'combined' were calculated, which relate to each of the terms in equations (5) and (6). The moments of the main wing and body section were output directly from the CFD simulations. The tail forces in the directions shown in Figure 8 ($F_{x_{vt}}$, $F_{y_{vt}}$, $F_{z_{vt}}$) were assumed to act at the tails' centres of pressure, and were multiplied by their respective moment arms about the aircraft centre of gravity in the longitudinal, vertical and horizontal directions (l_x, l_y, l_z) to give the corresponding tail moments (L_{vt}, M_{vt}, N_{vt}) [17] as presented in equations (8) to (10).

$$L_{vt} = \left(F_{y_{vt(p)}} - F_{y_{vt(s)}}\right) \cdot l_z - \left(F_{z_{vt(p)}} + F_{z_{vt(s)}}\right) \cdot l_y \tag{8}$$

$$M_{vt} = \left(F_{x_{vt(p)}} + F_{x_{vt(s)}}\right) \cdot l_y - \left(F_{y_{vt(p)}} + F_{y_{vt(s)}}\right) \cdot l_x \tag{9}$$

$$N_{vt} = \left(F_{z_{vt(p)}} + F_{z_{vt(s)}}\right) \cdot l_x + \left(F_{x_{vt(s)}} - F_{x_{vt(p)}}\right) \cdot l_z \tag{10}$$

The values of the moment arms differ for the inclined and vertical tails due to the larger size of the inclined tails and their angle of inclination. The values of the moment arms are presented in Table 4.

	Vertical configuration	Inclined configuration
l_x	16.85 m	16.67 m
l_y	4.69 m	4.52 m
l_z	13.00 m	14.83 m

Table 4: Tail moments arms aircraft about the aircraft centre of gravity at X=29.3m

The derivatives of the pitching, rolling and yawing moment coefficients with respect to sideslip and rudder angle were calculated using a three-point finite difference method with third order error terms [29], allowing unequal sub-intervals of sideslip and rudder angle to be used. When quoting the values of stability derivatives computed in this research, weighted averages are used because (i) the response of the aircraft is not linear giving rise to fluctuating

20

derivative values which need to be averaged and (ii) unequal intervals of rudder and sideslip angle were used in the CFD simulations. The weighted averages were calculated by integrating the moment coefficient derivative across the sub-intervals of rudder or sideslip angle and then dividing by the total interval range. This method has been repeated for the calculation of all averaged quantities stated in the results.

A linear response to an input would give constant values of stability derivative. Therefore, a smaller range or standard deviation of stability derivative corresponds to the response being closer to linear. The second derivative of moment coefficient also provides a measure of how predictable the aircraft response is to an input, with lower values of second derivative implying a more predictable response. These were calculated by reapplying the three-point finite difference method to the first derivatives of moment coefficient with respect to rudder or sideslip angle.

7.3. Stability in sideslip

The yawing moments at sideslip angles ranging from $1°$ to $15°$ are presented in Figures 9a and 9b for the vertical and inclined configurations. The general trend of 'combined' yawing moment is similar for each configuration; at $15°$ of sideslip they are equal to within 5.9%. This is due to both configurations having the same vertically projected area due to using the same vertical volume coefficient.

The averaged 'combined' values of yawing moment coefficient derivatives, C_{n_β}, for the aircraft model in both configurations are stated in Table 5. With both values of C_{n_β} being positive, this confirms that both configurations are directionally stable.

	Vertical configuration	Inclined configuration
C_{n_β} (rad^{-1})	0.091	0.093

Table 5: Averaged directional stability derivative values of the aircraft in vertical and inclined configurations

For both configurations, in Figures 9c and 9d, the values of C_{n_β} for the wing and body fluctuate only slightly in comparison with the tails. The correspondingly low range of C_{n_β} values, equal to 0.012, suggests that the response of the main wing and body is approximately linear. This is confirmed by the straight line relationship seen for the wing and body in Figures

9a and 9b. The values of C_{n_β} for a Boeing 747 aircraft [30] and an AC 20.30 twin-vertical-tail BWB [18] aircraft are also shown in Figures 9c and 9d, as these have a similar payload or design configuration respectively to the baseline model. The 'combined' average values of C_{n_β} for both the vertical and inclined configurations in Table 5 are lower than the Boeing 747 but larger than the AC 20.30. This indicates that both configurations have greater directional stability than the aforementioned AC 20.30 BWB model.

Referring to Figures 9a and 9b, the starboard tails gave larger restoring moments than the port tails for both configurations, except at $\beta = 15°$ for the vertical configuration. The stability of the starboard tails on both configurations reduces with sideslip angle, seen by their values of C_{n_β} tending to zero in Figures 9c and 9d. This is due to stall initiating first on the starboard tails between $\beta = 8°$ and $\beta = 10°$ where their response deviates from being linear in Figures 9a and 9b. This is confirmed in Figure 10 by the air recirculating at the trailing edge of the tail. This effect is less pronounced on the port tail of each configuration. Given the port tails are shielded by the main wing and body section, the 'angle of attack' at the port tails is less affected by an increase in sideslip which can be seen in Figure 10, thus prolonging stall.

In Figure 9a, there is a region of variation in combined yawing moment between $\beta = 1°$ and $\beta = 5°$ which is only present on the vertical configuration. This variation in moment is caused by fluctuations in the response of the port tail, seen in Figures 9a and 9c. The vertical port tail has been investigated but showed no discrepancies in pressure distribution between these angles of sideslip. Whilst the magnitudes of the yawing moments are always similar for the two configurations, the 'combined' response of the vertical configuration at sideslip angles less than 5° is less predictable, owing to its fluctuations in C_{n_β}.

Referring to Figures 9c and 9d, the 'combined' response for the inclined configuration is not linear but it does form a smoother curve than the vertical configuration; the maximum second derivatives of yawing moment coefficient with respect to sideslip at any point in the range are $0.37\ \mathrm{rad}^{-2}$ and $7.90\ \mathrm{rad}^{-2}$ for the inclined and vertical configurations respectively. These values have been calculated by reapplying the three-point finite difference method to the first derivatives of yawing moment coefficient with respect to sideslip. The region of fluctuation between 2° and 5° of sideslip for the vertical configuration accounts for its maximum second derivative value being greater than that of the inclined configuration. Larger second derivative values imply that if the

22

aircraft experiences a changing sideslip in flight, the corresponding change in yawing moment may suddenly be lower or higher than expected, affecting flight dynamics. Lower second derivative values and a smoother response makes the aircraft handling characteristics more predictable for the pilot. This means the pilot will find it easier to judge the response of the aircraft to a control surface input and they will also require fewer control surface inputs to retain the desired heading. The predictability of the stability derivative value throughout the range of sideslip angles allows the response to be easily modelled by a mathematical function. This means the dynamic stability of the aircraft can be modelled using closed-loop control more effectively, such as in the work of Neubacher [18].

For both configurations, the pitching moments of the whole aircraft were dominated by the negative (nose down) pitching moments of the main wing and body section. The pitching moments of the wing and body output from the CFD simulations, shown in Table 6, were greater in magnitude for the vertical than the inclined configuration by up to 190% at $\beta = 15°$. The tail pitching moments, calculated using equation (9), were found to have a negligible effect on the aircraft's pitching moment when analysing the vertical configuration. The tails of the inclined configuration gave an approximately linear increase in their magnitude of pitching moment with sideslip angle, but with opposite signs. At $\beta = 15°$, these equalled +2.3 MNm and -2.4 MNm for the port and starboard tails respectively. The tail moments combined to give a negative pitching moment which, on average, equalled 3% of the wing and body pitching moments. Therefore, the effect of the inclined tails on aircraft pitching moments could also be neglected.

Sideslip angle, $\beta°$	1	5	10	15
Vertical configuration (MNm)	-42.5	-40.5	-36.2	-29.8
Inclined configuration (MNm)	-22	-20.1	-15.8	-10.2

Table 6: 'Wing and body' section pitching moments with sideslip angle

The rolling moments of the aircraft wing and body become increasingly negative with sideslip angle for the vertical configuration, shown in Figure 11a. However, they become increasingly positive for the inclined configuration, as shown in Figure 11b, suggesting instability of the main wing and body section. This shows a high level of tail-body interaction as different trends are seen for the wing and body section's rolling moments with each

configuration of tail. Although it seems that the tails are required on the inclined configuration to keep the aircraft stable by causing the 'combined' values of rolling moment in Figure 11b to become negative, it is in fact the inclined tails which originally caused the instability of the wing and body.

In both configurations, the port and starboard tails give increasingly negative rolling moments with sideslip as shown in Figures 11a and 11b. However, the rolling moments of the inclined tails are greater in magnitude. Indeed, at β=15°, the rolling moment is more than double that of the vertical tails. For both tail configurations, it can be observed that the rolling moments of both the port and starboard tails follow a similar trend to their yawing moments, seen earlier in Figures 9a and 9b, except they have different sign and magnitude. This yaw-roll coupling is present since both of these moments are dependent on the horizontal tail forces but are multiplied by different moment arms.

The tail rolling moments are caused by horizontal and vertical forces, $F_{z_{vt}}$ and $F_{y_{vt}}$ respectively, as indicated in equation (8). The difference in tail rolling moments between the two configurations is partly due to the inclined starboard tail giving larger horizontal forces than the vertical starboard tail; 21% on average. However, the horizontally projected area of the inclined configuration creates large vertical forces, whereas these forces are negligible on the vertical configuration. Considering the inclined configuration, the ratio of vertical to horizontal forces averaged 0.4 and 0.42 for the port and starboard tails respectively. Despite the horizontal forces being larger than the vertical forces, the vertical forces are actually the dominating effect as their moment arm (l_z) is 3.28 times larger than the moment arm of the horizontal forces (l_y), obtained from Table 4.

The averaged 'combined' values of C_{l_β} are given in Table 7 for the inclined and vertical configurations. These values correspond to 1.83° and 2.53° of effective dihedral respectively [17]. As both values of C_{l_β} are negative and close to zero, the aircraft is stable with both configurations of tail, except at β=15° where the aircraft reaches marginal roll stability in both configurations. This can be seen in Figures 11c and 11d where the 'combined' C_{l_β} values reach zero.

The magnitudes of the averaged C_{l_β} values are low in comparison to those of a Boeing 747 or the AC 20.30. For example, the C_{l_β} value of the vertical configuration is only 20% of that of the Boeing 747, the value of which can be seen in Figures 11c and 11d. Therefore the C_{l_β} value of the inclined configuration, which is greater in magnitude than the vertical configuration

	Vertical Configuration	Inclined Configuration
C_{l_β} (rad^{-1})	-0.021	-0.029

Table 7: Averaged lateral stability derivative values of the aircraft in vertical and inclined configurations

by 38% (see Table 7), is preferable in order to give a greater margin of safety from entering the spiral mode which would be exhibited if the C_{l_β} value was greater than zero. Although suggested that C_{l_β} be around a half of C_{n_β} in magnitude [17], this ratio is only 0.31, even for the more stable inclined configuration. The values of C_{l_β} could be increased by mounting the tails further outboard; this would increase the moment arm of vertical forces, though may be impractical due to lack of mounting location on the wing section. The taper ratio of the tails could be increased in order to move the centre of pressure higher up the tail, therefore increasing the vertical moment arm of horizontal forces.

7.4. Stability of rudder inputs

The averaged values of $C_{n_{\delta r}}$ for the aircraft in both configurations are given in Table 8. These values are both negative, implying stability. They are 115% and 92% greater respectively than that of the AC 20.30 BWB aircraft (the value of which can be seen in Figures 12c and 12d) implying a significantly sharper response to rudder inputs than the AC 20.30. Both the AC 20.30 and the baseline BWB model have far lower values of $C_{n_{\delta r}}$ than the Boeing 747, again shown in Figures 12c and 12d. Although data for only two BWB models is presented, it suggests that rudder inputs may be less responsive for BWB aircraft than traditional tube-and-wing configurations.

	Vertical Configuration	Inclined Configuration
$C_{n_{\delta r}}$ (rad^{-1})	-0.028	-0.025

Table 8: Averaged stability derivatives with rudder input of the aircraft in vertical and inclined configurations

The yawing moments with rudder angle for each configuration are presented in Figures 12a and 12b. At 30° rudder engagement the 'combined' yawing moments of each configuration are equal to within 2.2%. The inclined configuration is stable throughout the range of rudder angles as its

'combined' values of $C_{n_{\delta r}}$, shown in Figure 12d, are always negative. However, the starboard tail on the vertical configuration suffers from extreme variation in yawing moments once the rudder is engaged more than $8°$, seen in Figure 12a. For example, between $\delta_r = 20°$ and $23°$ the yawing moments produced by this tail reduce in magnitude by 44%. This causes the aircraft to become unstable, shown by positive values of 'combined' $C_{n_{\delta r}}$ at $\delta_r = 23°$ in Figure 12c.

In Figures 12a and 12b, the aircraft with inclined tails is closer to giving a linear relationship between yawing moment and rudder angle than the vertical configuration. This is due to the inclined configuration having a less fluctuating response; in Figures 12c and 12d the inclined configuration has a range of 'combined' $C_{n_{\delta r}}$ values which is only 25% of that for the vertical configuration. This is also confirmed by the standard deviation (S.D.) values of $C_{n_{\delta r}}$ for the port and starboard tails presented in Table 9, which are both lower for the inclined configuration. This makes the aircraft more predictable for the pilot to control with the use of rudder inputs. Figure 13 shows the pressure variations for each tail with $\delta_r = 10°$ along section A-A of the rudder leading edge, the position of which is highlighted in Figure 4. This value of rudder angle has been presented as it is the first position for which the response of any tail significantly deviates from a linear response in Figures 12a and 12b. The pressure variations show that the inclined tails produce a smoother pressure distribution with less scatter than the vertical tails, giving rise to their smoother, more linear response. The pressure distribution of the vertical starboard tail is the most erratic, which results in it having the largest standard deviation of $C_{n_{\delta r}}$ values as shown in Table 9. This erratic pressure distribution explains the sudden drop in the magnitude of yawing moment which the vertical starboard tail produces once the rudders are engaged to $10°$ and the severe fluctuations the tail then experiences as the rudder is engaged further. Ultimately, it is the vertical starboard tail which is responsible for the unpredictable response of the aircraft in its vertical configuration.

As shown in Figures 12a and 12b, for both configurations the port tail generally gives a more negative yawing moment than the starboard tail. As a positive rudder input moves towards port, the port-side rudder of each configuration moves in to cleaner air whereas the starboard rudder moves in to air which is heavily affected by the main wing and body. The velocity at the tails' suction side centre of pressure was recorded from the CFD simulation. For the vertical configuration, this velocity was on average 54% higher for the port tail than for the starboard tail, giving lower pressures and

26

| | S.D.($C_{n_{\delta r}}$) | |
Configuration	Port	Starboard
Vertical	0.023	0.034
Inclined	0.005	0.012

Table 9: Standard deviation of $C_{n_{\delta r}}$ values for individual tails in the range $1° \leqslant \delta_r \leqslant 30°$

greater lift. As can be seen in Figure 12a, the vertical port-side tail stalls at a rudder angle of 27° indicated by the values of yawing moment changing from negative to positive. In contrast, as seen in Figure 12b, the inclined configuration first experiences stall on the starboard tail at a rudder angle of 27°, but importantly delays the stall of the dominant port tail.

In Figure 12b, the inclined starboard tail at a sideslip angle less than 3° produces a positive yawing moment, which is in the opposite direction to what is expected. This is due to the two effects illustrated in Figure 14: (i) a region of low pressure, labelled 'A', on the inboard (pressure) side of the tail, which decreases with rudder angle as shown in Figures 14a and 14b; (ii) a region of low pressure, labelled 'B', on the outboard (suction) side of the tail, which increases in size as rudder angle is increased as seen in Figures 14c and 14d . For the starboard tails, the inboard side is the side which the rudder moves towards, so it is effectively the pressure side of the aerofoil. The changes in size of the pressure regions 'A' and 'B' are caused by the rudder engagement increasing aerofoil camber and therefore lift due to circulation around the aerofoil. The positive yawing moment of the inclined starboard tail at δ_r less than 3° is counteracted by the dominant port tail, making the sum of the yawing moments negative and retaining stability of the inclined configuration.

The rolling moments due to rudder engagement are now considered in order to understand how rudder control affects the lateral stability of the baseline aircraft. The rolling moments of the wing and body section, shown in Table 10, were low and positive for both configurations, always being less than +0.89MNm at any rudder angle. It can be seen by inspection of Table 10 that for each configuration the sum of the tail rolling moments, which indicates the total effect of the tails on the aircraft, was always positive (starboard wings down). At 1° rudder angle the tail rolling moments totalled +0.40MNm for the vertical tails and +0.43 MNm for the inclined tails, whilst

at 30° rudder angle they totalled +2.75MNm and +5.97MNm respectively. The vertical configuration performs better in this respect as rudder inputs cause less change in the roll axis. For example, when initiating a banked turn to port, the pilot would engage rudders to port before applying the ailerons to roll the port side wings down. Using the inclined configuration, the ailerons would have to produce a greater negative rolling moment to overcome the positive rolling moment of the tails.

	Rudder Engagement Angle (°)												
	1	2	3	5	8	10	12	15	18	20	23	27	30
	Vertical Configuration Rolling Moments (MNm)												
Wing & body	0.17	0.20	0.17	0.34	0.36	0.26	0.22	0.24	0.25	0.27	0.28	0.18	0.15
Port tail	0.20	0.24	0.29	0.40	0.50	0.62	0.76	0.83	1.00	1.05	1.20	1.34	0.80
Stbd tail	0.19	0.27	0.36	0.49	0.67	0.45	0.52	0.76	0.66	1.57	0.99	1.17	1.95
Combined	0.57	0.71	0.82	1.22	1.53	1.34	1.49	1.83	1.90	2.89	2.47	2.69	2.90
	Inclined Configuration Rolling Moments (MNm)												
Wing & body	0.59	0.60	0.11	0.33	0.23	0.19	0.19	0.22	0.42	0.15	0.18	0.25	0.89
Port Tail	1.10	1.24	1.42	1.40	1.70	2.18	2.56	2.48	2.94	2.89	3.07	3.25	3.64
Stbd Tail	-0.67	-0.52	-0.28	0.12	0.93	0.68	1.00	1.54	1.63	1.90	2.13	2.42	2.33
Combined	1.03	1.32	1.25	1.85	2.86	3.06	3.75	4.24	4.99	4.94	5.38	5.92	6.85

Table 10: Rolling moments (MNm) of each aircraft component with rudder angle

The pitching moments of the wing and body with rudder angle averaged -27.2 MNm for the vertical configuration and -27.8 MNm for the inclined configuration, which have been calculated from the values given in Table 11 using the averaging method described in Section 7.2. The pitching moments of the vertical tails given in Table 11 became increasingly positive with rudder angle, but were always negligible in comparison to the wing and body. Focusing on the inclined configuration presented in Table 11, the pitching moments of both tails were initially negative, totalling -1.32MNm. As the rudder angle increased, the starboard tail gave an approximately linear increase in pitching moment up to +1.84MNm at 30°. However, the port tail gave an increasingly negative pitching moment up to -1.95MNm at 30°. These moments cancelled at rudder angles above 20° to give a negligible effect on the aircraft wing and body pitching moments.

	Rudder Engagement Angle (°)												
	1	2	3	5	8	10	12	15	18	20	23	27	30
	Vertical Configuration Pitching Moments (MNm)												
Wing & body	-25.51	-25.44	-25.54	-25.64	-24.20	-27.43	-27.82	-34.36	-27.83	-27.10	-26.79	-25.79	-25.89
Port tail	0.02	0.03	0.03	0.02	0.05	0.05	0.07	0.12	0.15	0.19	0.26	0.40	0.54
Stbd Tail	0.19	0.20	0.21	0.23	0.28	0.27	0.29	0.35	0.38	0.43	0.50	0.59	0.66
Combined	-25.30	-25.22	-25.31	-25.39	-23.87	-27.12	-27.46	-33.89	-27.29	-26.48	-26.02	-24.80	-24.69
	Inclined Configuration Pitching Moments (MNm)												
Wing & body	-28.90	-28.94	-30.24	-31.12	-29.95	-25.48	-28.90	-29.29	-27.36	-29.45	-28.82	-27.77	-9.20
Port tail	-0.80	-0.89	-1.03	-0.96	-1.07	-1.43	-1.67	-1.48	-1.82	-1.66	-1.71	-1.75	-1.95
Starboard tail	-0.52	-0.42	-0.30	0.01	0.62	0.40	0.61	1.09	1.10	1.39	1.60	1.87	1.84
Combined	-30.22	-30.25	-31.57	-32.07	-30.40	-26.51	-29.96	-29.69	-28.08	-29.71	-28.93	-27.65	-9.30

Table 11: Pitching moments (MNm) of each aircraft component with rudder angle

8. Design assessment: Drag analysis

The vertical and inclined tail configurations have been analysed for their drag performance, via CFD simulation, at cruise conditions with an angle of attack of 4°, as the aircraft design lift coefficient of 0.41 was achieved at this angle [1]. The drag for the whole aircraft in each configuration is presented in the rightmost column of Table 12. This is obtained from the sum of the drag due to each component: the wing and body only (middle column) and the starboard and port tails combined (leftmost column). Theses values have been further decomposed in to skin drag and pressure drag by recording the skin friction and pressure forces in the freestream direction for each component from the CFD simulations.

Drag source	Tails only		Wing & Body		Whole aircraft	
(kN)	Vertical	Inclined	Vertical	Inclined	Vertical	Inclined
Skin Drag	5.43	6.25	60.94	60.57	66.36	66.82
Pressure Drag	10.74	12.80	350.43	398.44	361.17	411.24
Total Drag	16.17	19.05	411.37	459.02	427.54	478.06

Table 12: Drag components for inclined and vertical configurations at $\alpha = 4°$

The total drag of the whole aircraft was 11.8% greater in the inclined configuration than in the vertical configuration. As can be determined from the leftmost column of Table 12, the total drag of the inclined tails is only 17.8% greater than the vertical tails alone. This can be partially attributed to the inclined tails having a 7.9% larger side view area than the vertical

tails. However, the inclined tails gave a greater drag coefficient of 0.0098 compared with 0.0090 for the vertical tails. These drag coefficients were calculated using the total drag of the tails indicated in Table 12 and the reference area was taken to be twice the tail area, S_{vt}, of each configuration due to there being two tails present.

The pressure drag of the wing and body section was 13.7% greater in the inclined configuration than in the vertical configuration. As the drag of the wing and body section is considerably greater than that of the tails alone for either configuration, increasing the pressure drag of the wing and body has a significant effect on the total drag of the aircraft. The inclined configuration therefore performs worse than the vertical configuration in terms of drag, partially because its tails experience higher drag themselves, but also because they interact with the wing and body to increase its pressure drag.

9. Conclusion

Vertical stabilisers applied to a blended wing body aircraft have been analysed for their stability with respect to sideslip and rudder inputs. A computational BWB aircraft model with vertical and inclined twin-stabiliser designs has been generated. The volume coefficient method has been used to aid the design of the tails whilst keeping their dimensions in proportion to those of the A380. CFD software was initially used to perform a 'mock' asymmetric thrust test on the computational BWB aircraft model revealing that the volume coefficient for the BWB model could be as low as 0.02417, which is 40.5% of that used on the Airbus A380. Consequently, vertical stabilisers were deemed as being feasible for use on BWB aircraft as they do not need to be excessively large, providing they are used in a twin-tail configuration.

In all of the analyses conducted with respect to sideslip and rudder angle, the BWB aircraft modelled proved to be directionally stable in both the inclined and vertical twin-tail configurations. The average derivative values of yawing moment coefficient with respect to sideslip and rudder angle obtained were similar for the inclined and vertical configurations of stabilisers. However, the inclined configuration gave a more predictable response with respect to both sideslip and rudder engagement as its stability derivatives had a lower range and standard deviation than the vertical configuration. The tails of the inclined configuration produced larger rolling moments with both sideslip and rudder angle than those of the vertical configuration. This

was an advantage of the inclined tails in sideslip as they increased the lateral stability of the aircraft by 38% when compared with the vertical tails. However, this was a disadvantage with respect to rudder inputs as the inclined tails increased the adverse yaw-roll coupling. Further work could be conducted to take the static stability derivatives found in this research and apply them to dynamic stability and control analysis. This would require an estimation of the payload distribution in order to calculate the moments of inertia of the aircraft.

The inclined configuration performed worse in terms of drag as it increased the pressure drag of the aircraft's wing and body by 13.7% when compared with the vertical configuration. The presence of the inclined tails also created more drag than the vertical tails, partially due to their larger drag coefficient and also due to their side area being larger.

This research has established that vertical stabilisers are a feasible option to provide directional stability for a BWB aircraft, though they must be used in a twin-tail configuration due to size limitations. Furthermore, this confirms that BWB aircraft need not be tailless as other authors have previously suggested. The inclined tails had negative effects on the aircraft drag. However, the tails are advised to be mounted in an inclined configuration on BWB aircraft to make their yaw response to sideslip and rudder inputs more predictable thus aiding controllability of the aircraft.

[1] Qin, N. et al. (2004). Aerodynamic considerations of blended wing body aircraft. Progress in Aerospace Sciences, 40(6):321-343.

[2] Dassault Systems, (2015). Solidworks 3D CAD. [Computer program].

[3] Turner, A. et al. (2009). Meeting the UK aviation target - options for reducing emissions to 2050. Committee on Climate Change, p. 12.

[4] G. Norris, M. Wagner, (2010). Superjumbo of the 21st century, Zenith press.

[5] The Boeing Company, (2014). Boeing 2014 Environment Report, pp. 14-16.

[6] Federal Aviation Administration, (2014). AC150/5300-13A Airport Design, p. 14.

[7] Clean Sky (2015). Aviation and Environment. Available from: http://www.cleansky.eu/content/homepage/aviation-environment.

[8] Aviation Archive: Aviation Heritage, (2004). Westland Dreadnought. Available from: http://www.aviationarchive.org.uk/Gpages/html/G3806.html.

[9] Flight Global Archive, (1938). Flight Magazine April 21st 1938, pp. 378.

[10] Liebeck, R., The Boeing Company, (2004). Design of the Blended Wing Body Subsonic Transport, Journal of Aircraft, 41(1):10-25.

[11] Kozek, M., Schirrer, A., (2015). Modeling and Control for a Blended Wing Body Aircraft: A Case Study, Vol.145 (Advances in Industrial Control). Springer International Publishing.

[12] Hepperle, M., German Aerospace Centre (DLR), (2005). The VELA Project. Available from: http://www.dlr.de/as/en/Portaldata/5/Resources/dokumente/projekte /vela/The_VELA_Project.pdf.

[13] Cambrige-MIT Instiute, (2006). Silent Aircraft Initiative. Available from: http://silentaircraft.org/sax40.

[14] European Commission, (2012). Final Report Summary - NACRE (New aircraft concepts research). Available from: http://cordis.europa.eu/result/rcn/53021_en.html.

[15] European Commission, (2012). ACFA 2020 Active Control of Flexible 2020 Aircraft. Available from: http://ec.europa.eu/research/transport/projects/items/acfa_2020_en.html.

[16] Lehmkeuhler, K., Wong, K., and Verstaete, D., (2012). Design and Test of a UAV Blended Wing Body configuration. 28th International Congress of the Aeronautical Sciences, p. 6.

[17] Raymer, D., (2005). Aircraft Design: A Conceptual Approach. 4th ed. American Institute of Aeronautics and Astronautics, Inc..

[18] Neubacher, C., (2008). Flight Dynamic Investigations of a Blended Wing Body Aircraft. PhD thesis, Hamburg University of Applied Sciences.

[19] Ordoukhanian, E. and Madni, A., (2014). Blended Wing Body Architecting and Design: Current Status and Future Prospects. 2014 Conference on Systems Engineering Research, Vol. 28, pp. 619-625.

[20] Creech, G., National Aeronautics and Space Administration, (2010). Back in the Air: X-48B Resumes Flight Tests at NASA Dryden. Available from: http://www.nasa.gov/centers/dryden/status_reports/X-48B_status_09_21_10.html.

[21] Creech, G., National Aeronautics and Space Administration, (2013). X-48 Research: All good things must come to an end. Available from: http://www.nasa.gov/topics/aeronautics/features/X-48_research_ends.html.

[22] Sobachkin, A., Dumnov, G., Dassault Systems, (2014). Numerical Basis of CAD-Embedded CFD: White paper.

[23] Balakin, V., Churbanov, A., Gavriliouk, V., Makarov, M. and Pavlov, A., (2004). Verification and Validation of EFD.Lab Code for Predicting Heat and Fluid Flow. Proceedings of ICHMT International Symposium on Advances in Computational Heat Transfer, Norway, April 19-24, 2004.

[24] Jenkinson, L., Simpkin, P. and Rhodes, D., (1999). Civil Jet Aircraft Design. Elsevier Limited.

[25] Sadreay, M., (2012). Aircraft Design: A Systems Engineering Approach. Wiley Publications.

[26] European Aviation Safety Agency, (2007). CS 25.149 Minimum Control Speed. In CS-25 Certification Specifications for Large Aeroplanes Amendment 3.

[27] AIRBUS S.A.S.. Airbus A380 Certification Objectives. Available from: www.aci.aero/media/b9137bb7-a2de-405f-8eb9-be0013515e96/.

[28] Federal Aviation Administration, (2009). FAA Type Certificate Data Sheet NO. A58NM, A380-800 Series Transport Category Airplanes.

[29] Singha, A. and Bhadauria, B. (2009). Finite Difference Formulae for Unequal Sub-Intervals Using Lagranges Interpolation Formula. Int. Journal of Math. Analysis, 3(17):815-827.

[30] Caughey, D., (2011). Chapter 5.4 Stability Characteristics of the Boeing 747. In Introduction to Aircraft Stability and Control Course Notes for M&AE 5070.
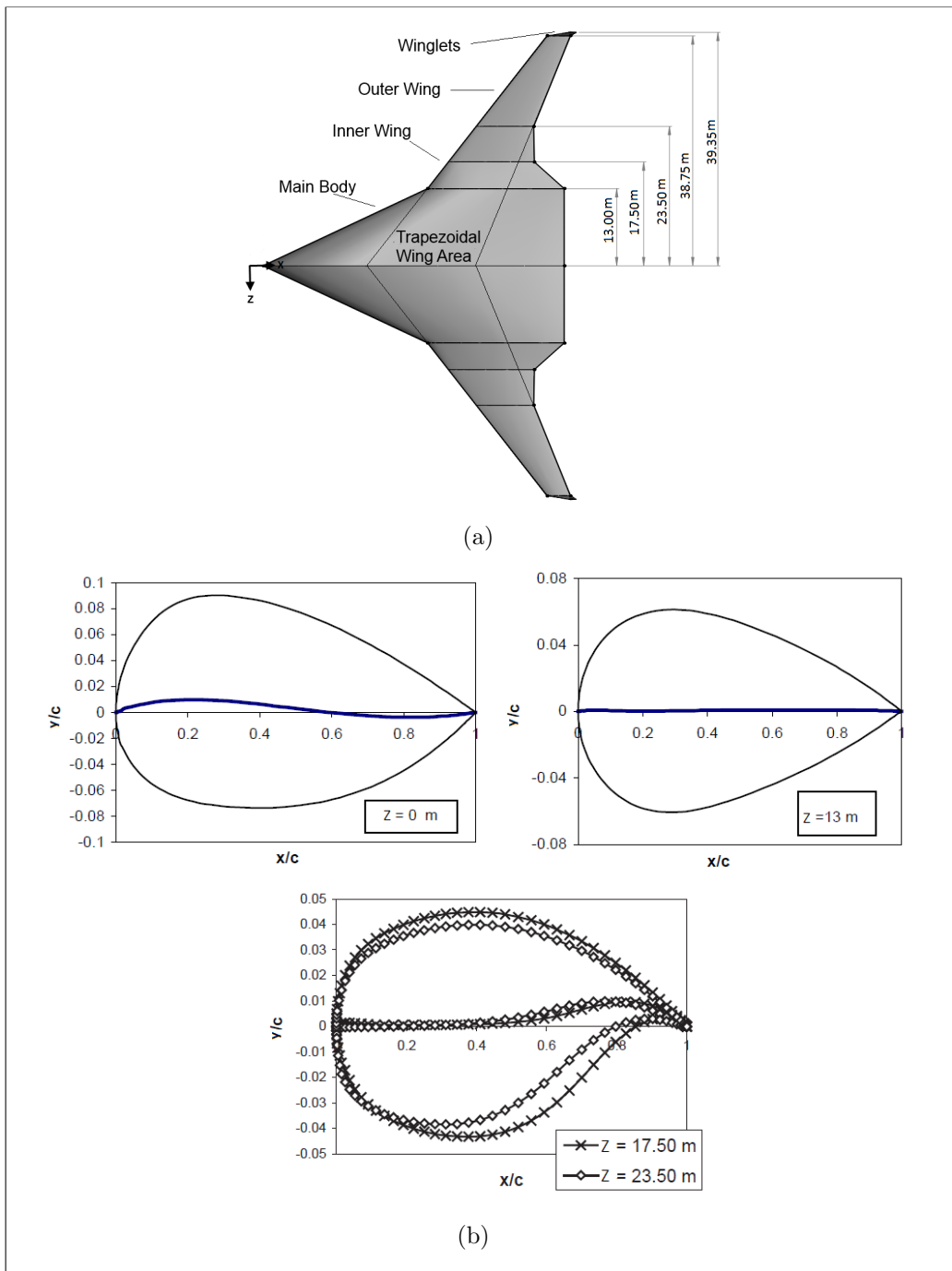
Figure 1: (a) Planform geometry of baseline model in x-z plane and (b) camber and thickness distributions for aerofoil sections [1].
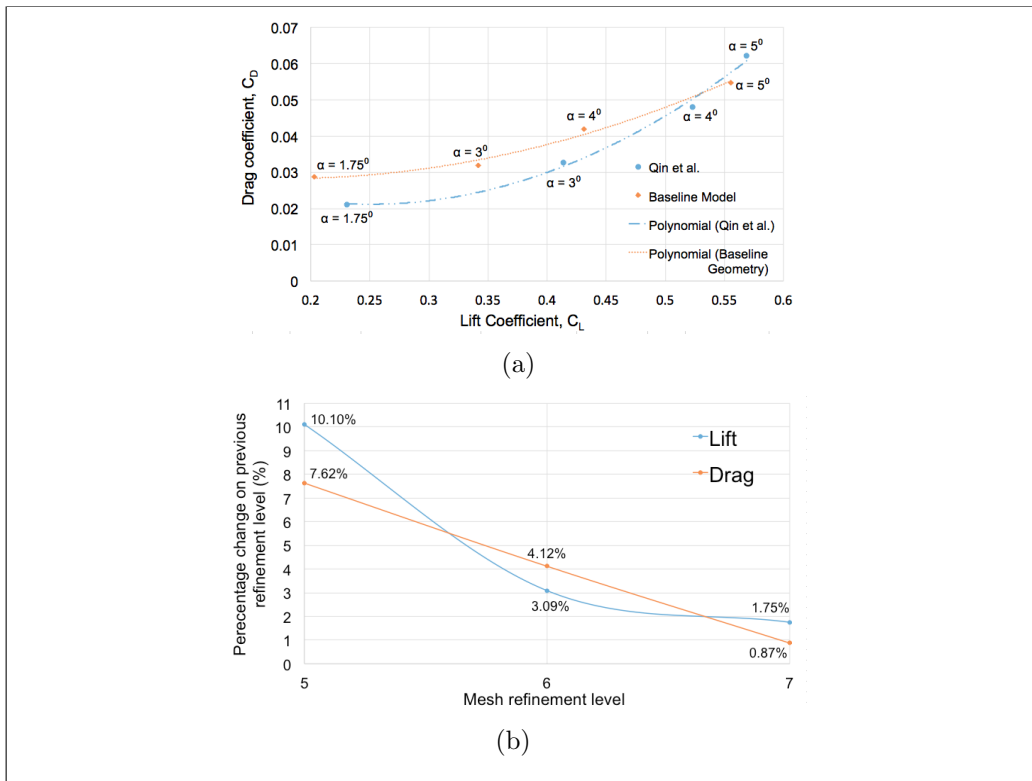
Figure 2: (a) Lift and drag polar for the baseline model and Qin et al.'s model [1] and (b) change in lift and drag with mesh refinement level for baseline model.
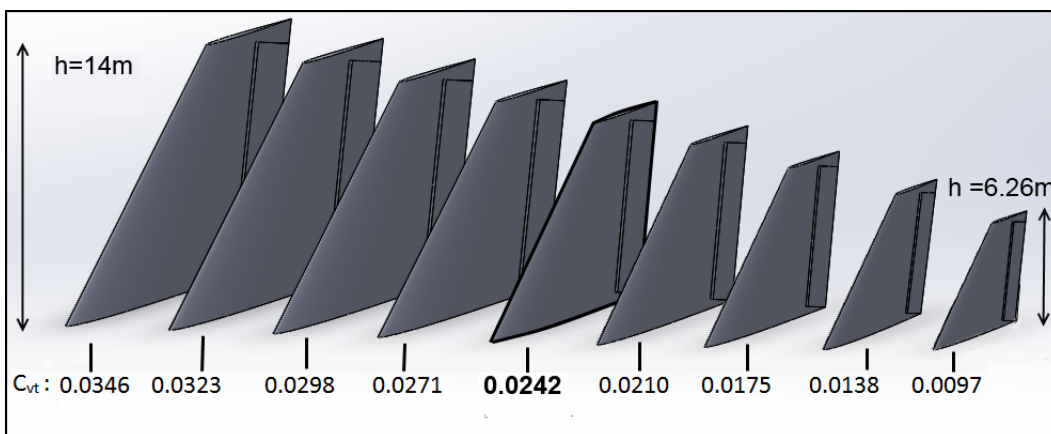
Figure 3: Family of vertical tails with varying volume coefficient
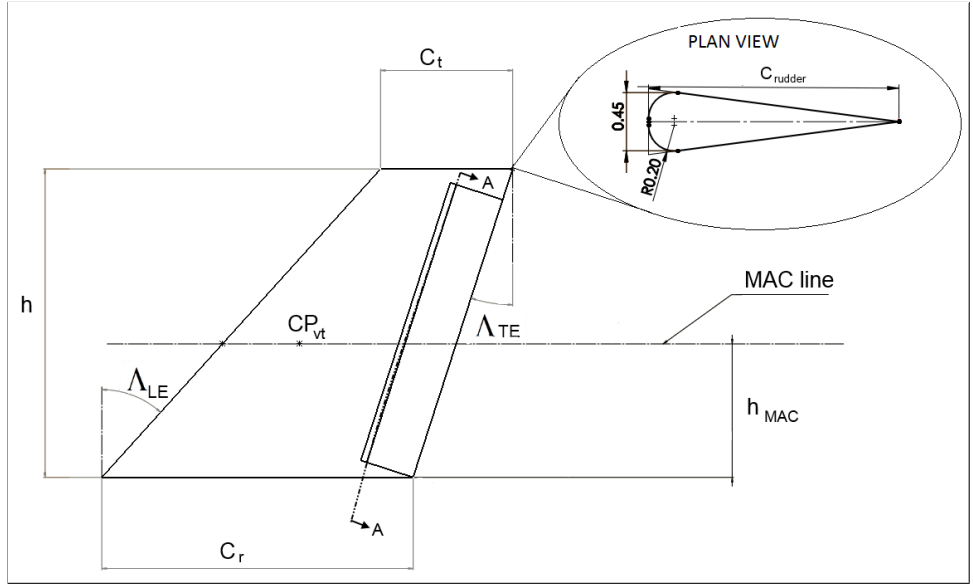
Figure 4: Design parameters of a vertical tail - side view
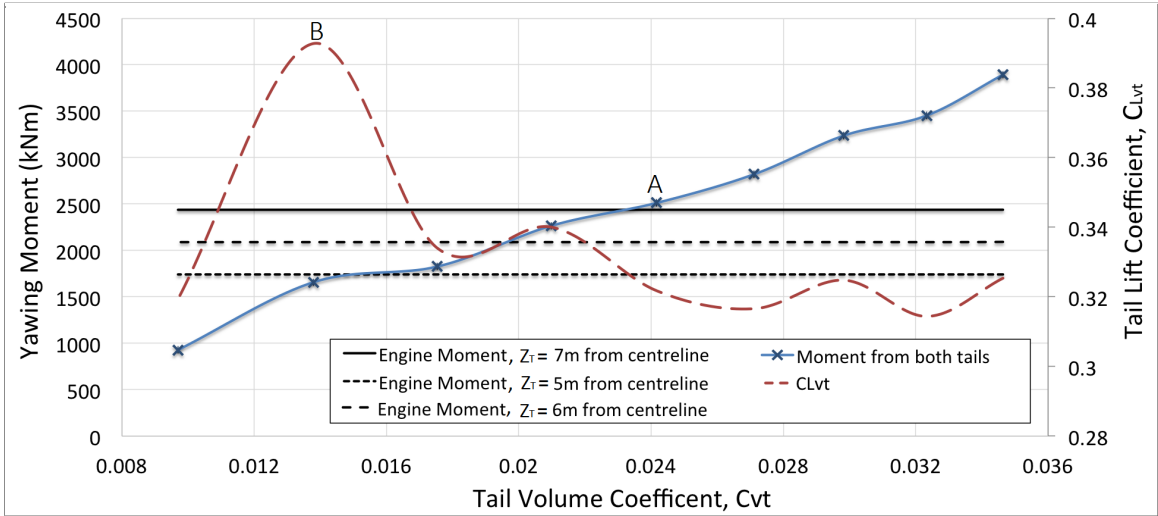
Figure 5: Asymmetric thrust testing with $\delta_r = 30°$
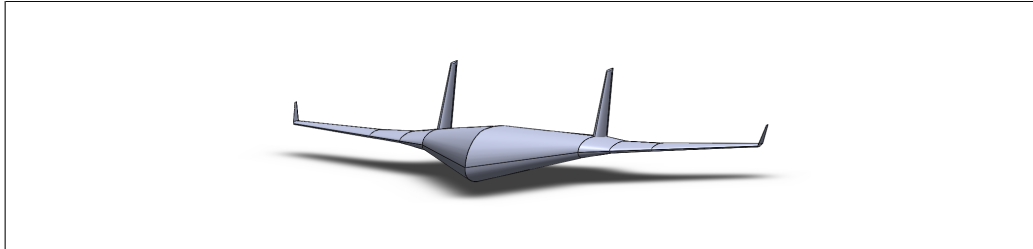
Figure 6: Baseline model with vertically mounted twin-stabilisers
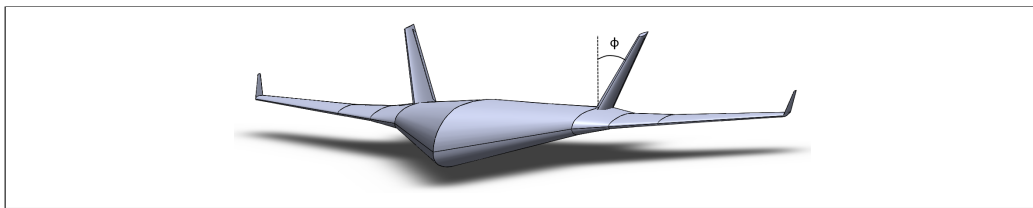
Figure 7: Baseline Model with inclined mounted twin-stabilisers
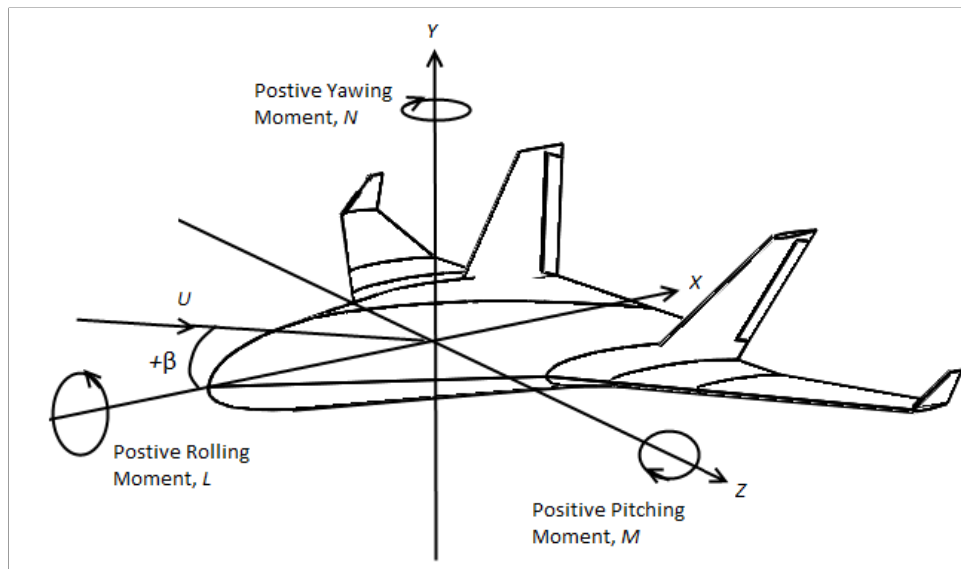
Figure 8: Positively defined aerodynamic moments and cartesian axes
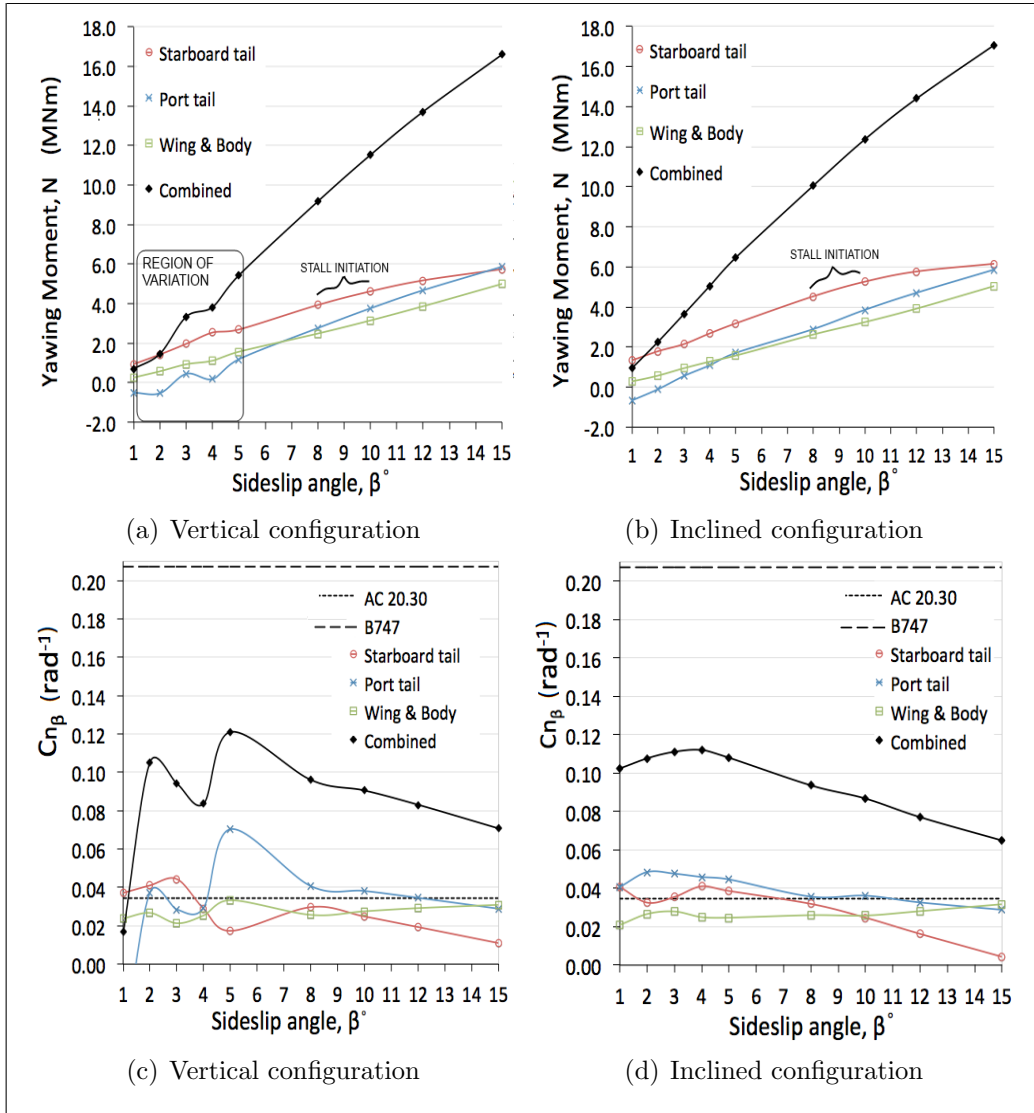
Figure 9: (a)-(d) Yawing moments and C_{n_β} with sideslip angle for vertical and inclined configurations.
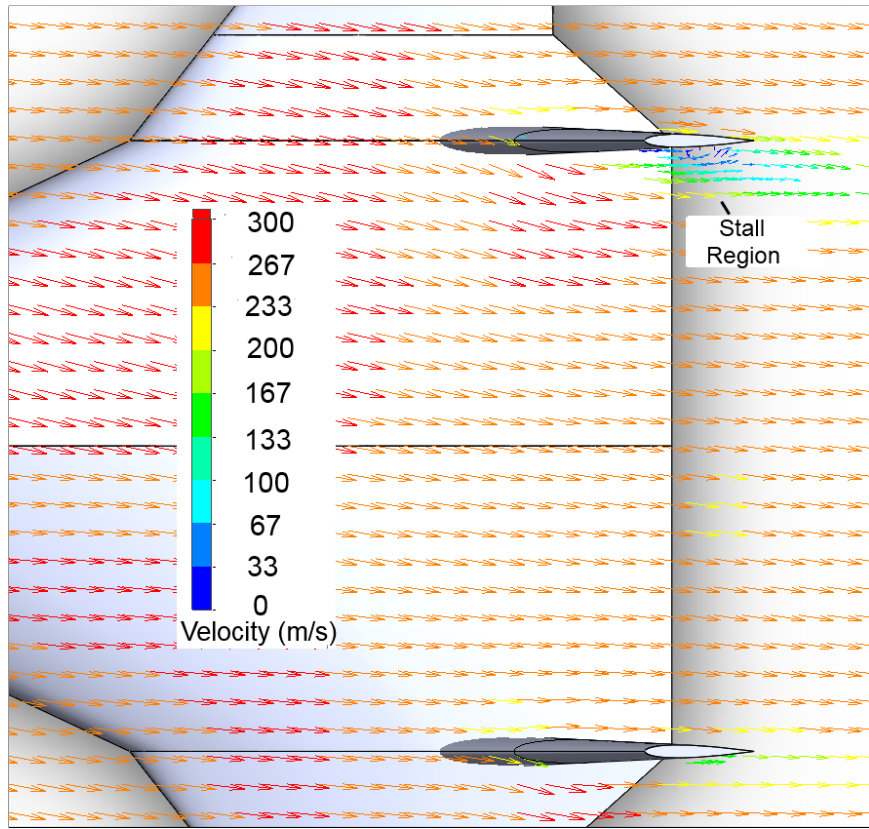
Figure 10: Vertical configuration - Velocity vectors at tail MAC height with $\beta = 10°$

(a) Vertical configuration
(b) Inclined configuration
(c) Vertical configuration
(d) Inclined configuration
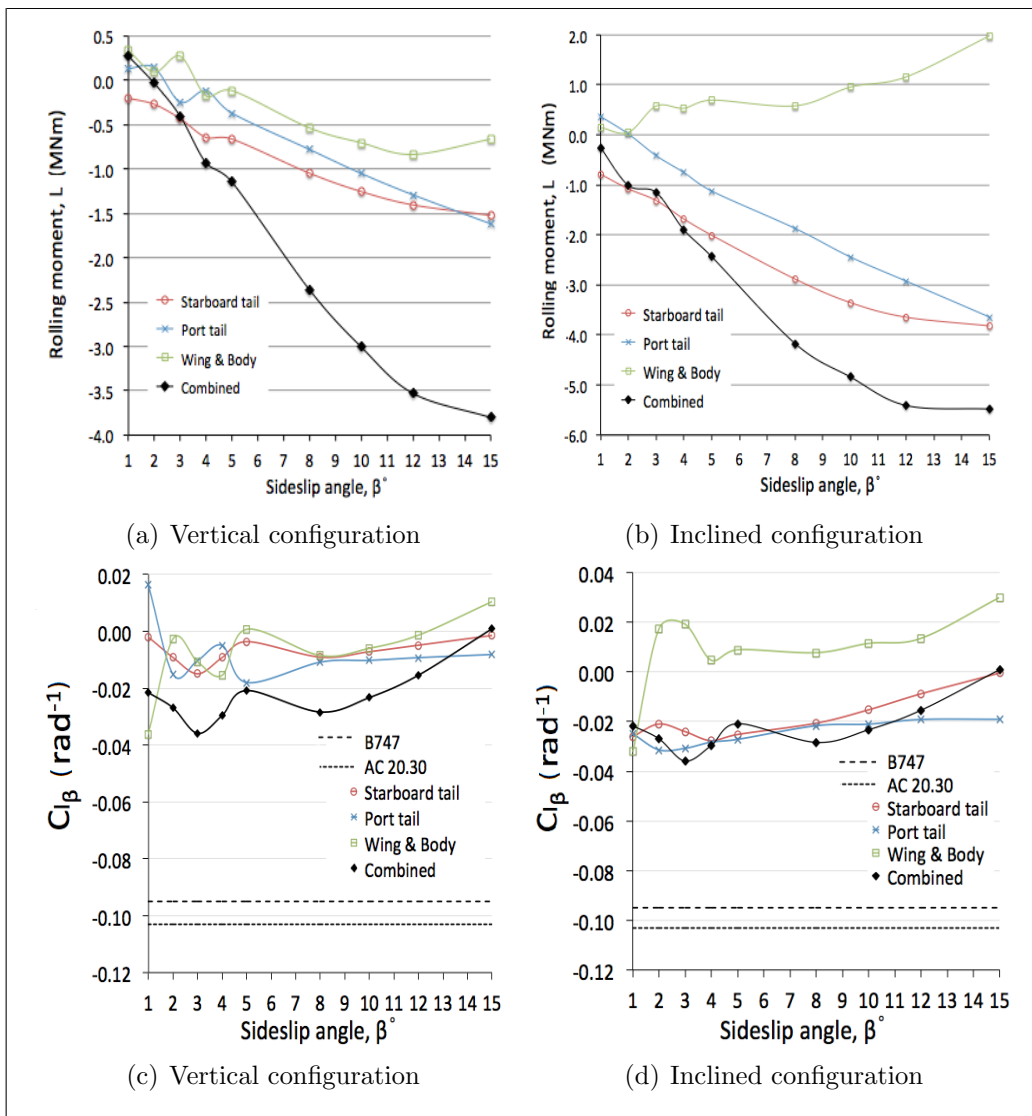
Figure 11: (a)-(d) Rolling moments and C_{l_β} with sideslip angle for vertical and inclined configurations.
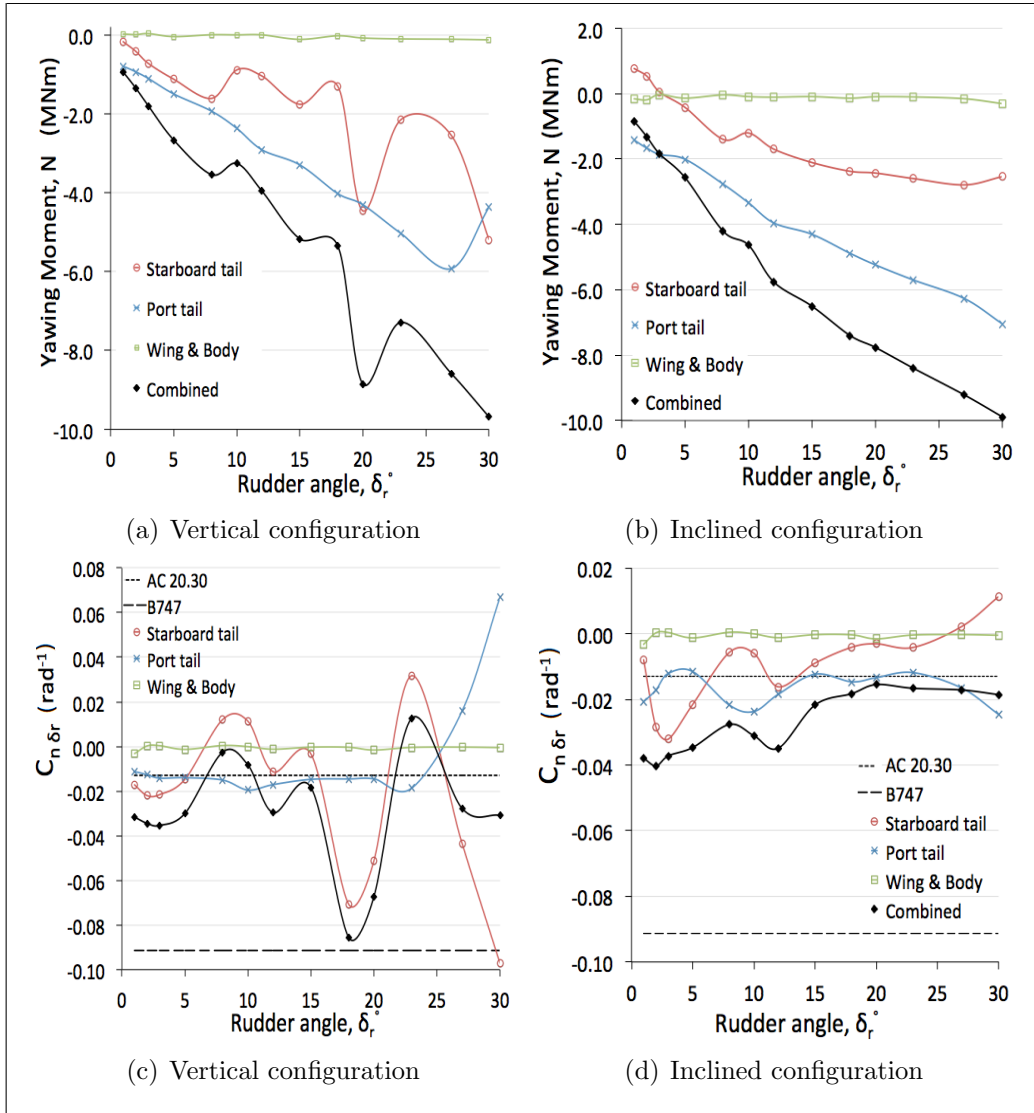
Figure 12: (a)-(d) Yawing moments and $C_{n_{\delta r}}$ with rudder angle for vertical and inclined configurations.
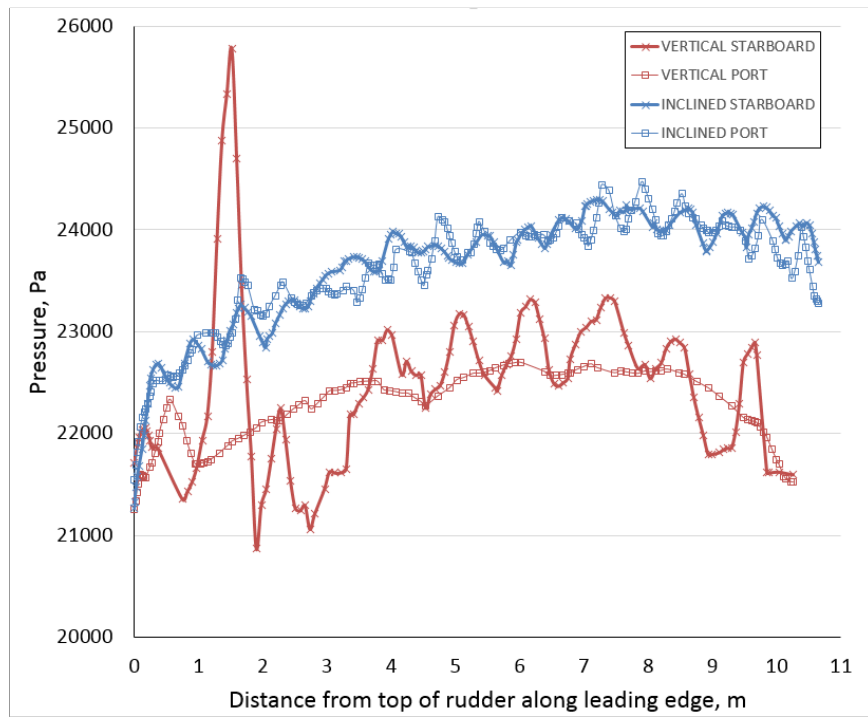
Figure 13: Pressure distributions along section A-A at leading edge of rudder with $\delta_r = 10°$

(a) Inboard $\delta_r = 1°$ (b) Inboard $\delta_r = 5°$

(c) Outboard $\delta_r = 1°$ (d) Outboard $\delta_r = 5°$
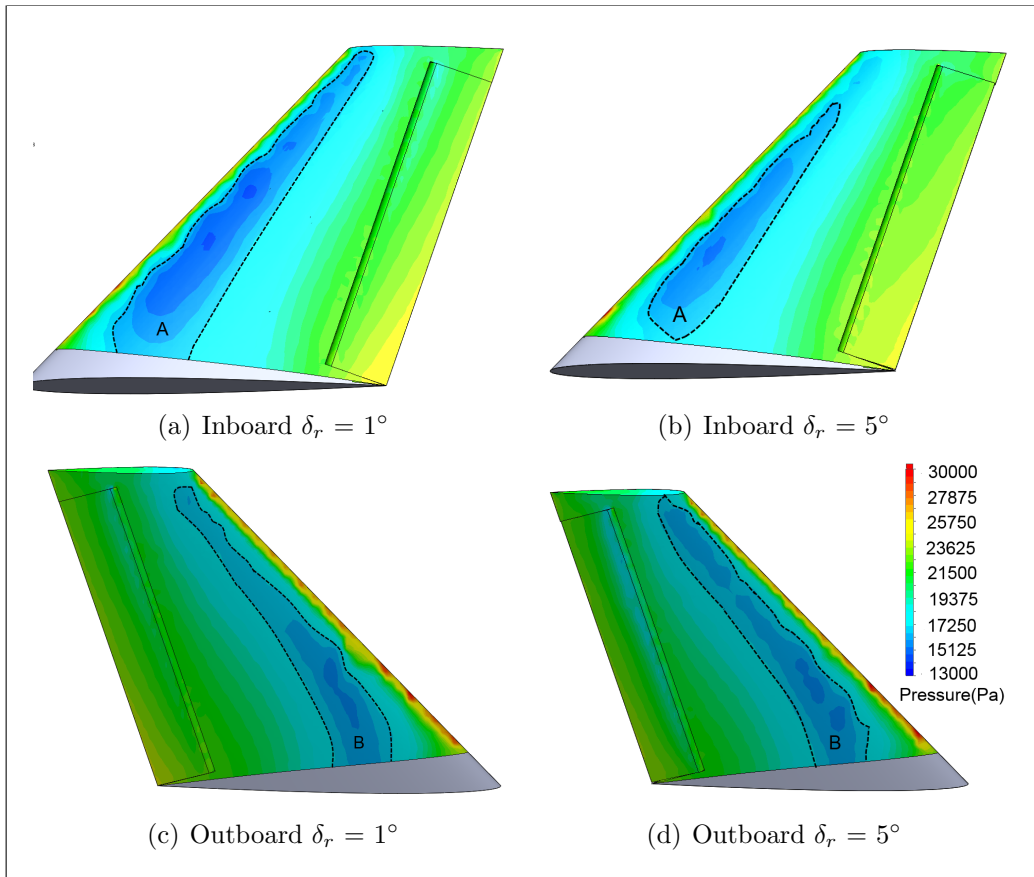
Figure 14: Pressure plots of the inclined starboard tail